PCCP

PAPER

View Article Online
View Journal | View Issue

Cite this: *Phys. Chem. Chem. Phys.*, 2014, **16**, 5755

Insights into the active surface species formed on Ta_2O_5 nanotubes in the catalytic oxidation of CO

Renato V. Gonçalves,*[a] Robert Wojcieszak,[a] Paula M. Uberman,[a] Sergio R. Teixeira[b] and Liane M. Rossi*[a]

Received 19th November 2013,
Accepted 29th January 2014

DOI: 10.1039/c3cp54887b

www.rsc.org/pccp

Freestanding Ta_2O_5 nanotubes were prepared by an anodizing method. As-anodized amorphous nanotubes were calcined at high temperature to obtain a crystalline phase. All materials were studied by means of BET analysis, XRD, TEM, SEM, XPS, and FTIR and were evaluated in the catalytic oxidation of CO. An XPS study confirmed the formation of different tantalum surface species after high temperature treatment of amorphous Ta_2O_5 nanotubes. Calcination at 800 °C generated Ta^{4+} while higher temperature (1000 °C) treatment led to the formation of Ta^{3+} species. These materials also showed significant differences in catalytic activity. Higher activity was observed for samples calcined at 800 °C than at 1000 °C, suggesting that Ta^{4+} species are active sites for CO oxidation.

1 Introduction

Tantalum pentoxide (Ta_2O_5) is one of the most active photocatalysts for water splitting under UV irradiation.[1–3] It has also received attention as a starting material for the synthesis of different photocatalytically active catalysts ($NaTaO_3$, $KTaO_3$, and $LiTaO_3$).[4–6] The high photocatalytic activity of Ta_2O_5 probably arises from its surface structure and bulk electron diffusion lengths that together generate more surface-active catalytic sites than are seen in other semiconductors.[2,7] Several studies have examined the application of bulk Ta_2O_5 as an active heterogeneous catalyst.[8–10] However, to the best of our knowledge, no studies have shown the use of Ta_2O_5 nanotubes (Ta_2O_5 NTs) in heterogeneous catalysis, although the use of other semiconductor oxides (*e.g.*, TiO_2) as catalyst supports has been widely covered in the literature. In general, these show relatively high catalytic activities for CO oxidation.[11,12]

The support structure is also known to play a leading role in the catalytic process.[13,14] Recently, Somorjai *et al.* found a strong correlation between the oxidation state of the oxide support and the catalytic activity.[15] Motivated by the high potential for applications of Ta_2O_5, we have prepared Ta_2O_5 NTs and investigated their fundamental structure and physicochemical properties. In this study, Ta_2O_5 NTs were prepared by an anodization method.[2] Several studies have already reported on the photocatalytic properties of these materials, so we focused on the catalytic oxidation of CO. The aim of the present study was to prepare amorphous and crystalline Ta_2O_5 NTs and to demonstrate their morphology-dependent catalytic activity. The Ta_2O_5 NTs presented here show a lower temperature for CO oxidation activity than is seen with CeO_2 and CeO_2–Al_2O_3 (ref. 16) mixed nano-powders, which have been widely studied as CO oxidation catalyst supports. This indicates that Ta_2O_5 NTs have high potential for application as a catalyst material.

2 Experimental

2.1 Preparation of catalysts

Ta_2O_5 NTs were prepared by anodizing high-purity Ta discs (3 cm of diameter, 99.9%) in an electrolyte consisting of 1 vol% of hydrofluoric acid (HF, 40%), 4 vol% deionized water (H_2O-DI), and sulfuric acid (H_2SO_4, 98%) as the solvent at a voltage of 50 V at 50 °C for 20 min.[2] Immediately after the anodization process, the prepared NTs were collected in a receptacle with water and decanted. Afterwards, the water was removed and the obtained white powder was dried in air. The NTs were calcined in a muffle furnace under atmospheric air at different temperatures, at a heating rate of 5 °C min^{-1}. The catalytic activity of the prepared materials was compared to a commercial nanopowder of Ta_2O_5 (99.98%) purchased from Sigma Aldrich.

2.2 Characterization of Ta_2O_5 NTs

Microscopy analysis. A scanning electron microscope (FESEM, FEI Inspect F50) and a transmission electron microscope (JEOL JEM1200 EXII – LNLS 13057) were used to observe the morphology of the freestanding Ta_2O_5 NTs.

[a] *Laboratory of Nanomaterials & Catalysis, Institute of Chemistry, USP, Av. Professor Lineu Prestes, 748, São Paulo, 05508-000 SP, Brazil. E-mail: rsvg12@iq.usp.br, lrossi@iq.usp.br*
[b] *Institute of Physics, UFRGS, Av. Bento Gonçalves 9500, Rio Grande do Sul 15051 RS, Brazil*

X-ray diffraction. The crystal structures were analyzed by X-ray powder diffraction (XRD). The diffraction patterns were recorded on a Philips X'PERT diffractometer with Cu Kα radiation (λ = 1.54 Å) at 2θ = 5–100° with a 0.02° step size and measuring time of 5 s per step. Rietveld refinement procedures were applied for the crystal structure analysis using Fullprof software.[17]

Specific surface area. Specific surface area (S_{BET}) was measured according to the Brunauer–Emmett–Teller method (BET) using nitrogen absorption isotherms obtained on a Micromeritics TriStar II 3020 apparatus. The samples were degassed overnight at 150 °C under vacuum prior to nitrogen adsorption measurements.

X-ray photoelectron spectroscopy. X-ray photoelectron spectra (XPS) were obtained using conventional equipment equipped with a high-performance hemispheric SPECSLAB II (Phoibos-Hs 3500 150 analyzer, SPECS, 9 channels) energy analyzer and non-monochromatic Al Kα ($h\nu$ = 1486.6 eV) radiation as the excitation source. The operating pressure in the ultrahigh vacuum chamber (UHV) during analysis was 10^{-7} Pa. Energy steps of 50 and 20 eV were used for the survey and single-element spectra, respectively. Peak decomposition was performed using curves with a 70% Gaussian type and a 30% Lorentzian type, and a Shirley nonlinear sigmoid-type baseline. The following peaks were used for the quantitative analysis: O1s, C1s, and Ta4f. The S2p and F1s peaks were also monitored and C1s was monitored again to check for charge stability as a function of time. Molar fractions were calculated using peak areas normalized on the basis of acquisition parameters after a Shirley background subtraction and corrected with experimental sensitivity and transmission factors provided by the manufacturer. The C–(C, H) component of the C1s peak of adventitious carbon was fixed to 284.8 eV to set the binding energy scale, and the data treatment was performed using CasaXPS software (Casa Software Ltd., U.K.).

FTIR studies. Infrared measurements were performed on an IRPrestige-21 Shimadzu FTIR spectrometer. One milligram of the sample was dispersed in a KBr pellet with slight grinding for FTIR measurements at room temperature. The spectra were collected in the 400–4000 cm^{-1} range for all materials. A pure KBr pellet was used as the background for all measurements and its spectrum was automatically subtracted from the FTIR spectra.

2.3 Catalytic CO oxidation

The catalytic CO oxidation experiments were performed using 20 mg Ta_2O_5 NT powder placed in a quartz tube reactor (length: 20 mm, width: 5 mm). The reaction temperature was controlled by a temperature sensor on the Integrated Microreactor-MS with CATLAB-PCS Module & QIC-20 MS Module. A continuous flow of the reactant mixture containing 1.75 vol% CO, 7 vol% O_2, and Ar balance was passed through the reactor at a total flow rate of 100 mL min^{-1}.

3 Results

3.1 Freestanding Ta_2O_5 nanotubes.

Fig. 1 shows FESEM and TEM images of tantalum oxide nanotubes prepared by anodization of tantalum foil in an aqueous electrolyte containing H_2SO_4 + 1 vol% HF + 4 vol% H_2O at 50 V.[2] Anodization was carried out for 20 min at 50 °C. The surface morphology of the as-anodized Ta_2O_5 NTs, as shown in Fig. 1(a) and (b), is a nanotubular structure with an average inner diameter of ~50 nm, wall thickness of ~30 nm and length of ~5 μm. The as-anodized NTs have continuous smooth walls and are open at the top and closed at the bottom. The NTs calcined at 800 °C for 30 min (Fig. 1(c) and (d)) have similar morphology to that of the as-anodized material.

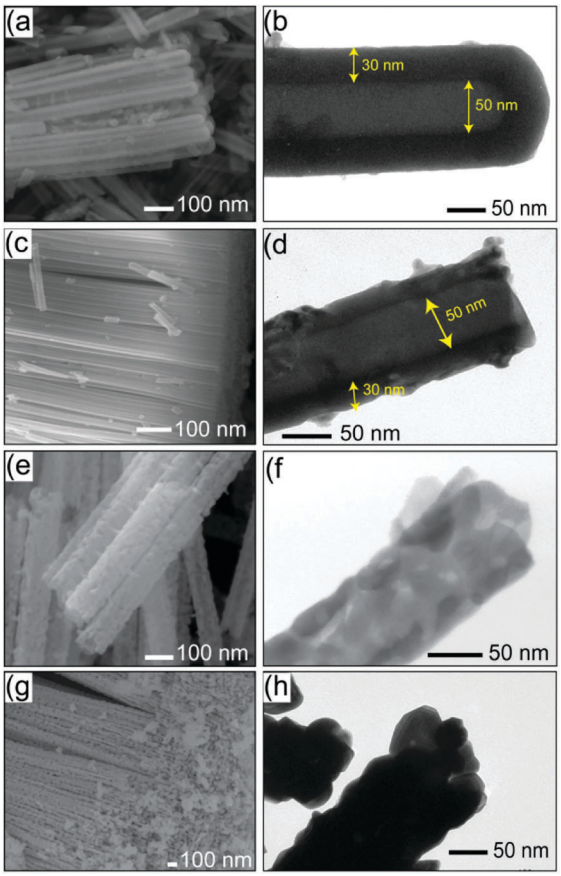

Fig. 1 FESEM and TEM images of the top view and cross-section of freestanding Ta_2O_5 NTs: (a and b) as-anodized, (c and d) calcined at 800 °C and (e and f) calcined at 800 °C for 60 min and (g and h) calcined at 1000 °C.

The Ta_2O_5 NTs calcined at 800 °C for 60 min (Fig. 1(e) and (f)) have rough walls with small crystals and holes in the nanotubular structure. However, the overall tubular structure was unaffected. Increasing the temperature of calcination to 1000 °C (Fig. 1(g) and (h)) completely destroyed the tubular structure. At this temperature, the NT walls were converted into crystal particles with an average size of ~60 nm.

3.2 Crystalline structure

The crystalline structure of as-anodized and calcined NTs was analyzed by XRD. The as-anodized Ta_2O_5 NTs have an amorphous structure, as previously reported.[2,18] Fig. 2 shows the XRD patterns and Rietveld refinements of the as-anodized Ta_2O_5 NTs, calcined at 800 and 1000 °C, and the commercial sample. The refinement

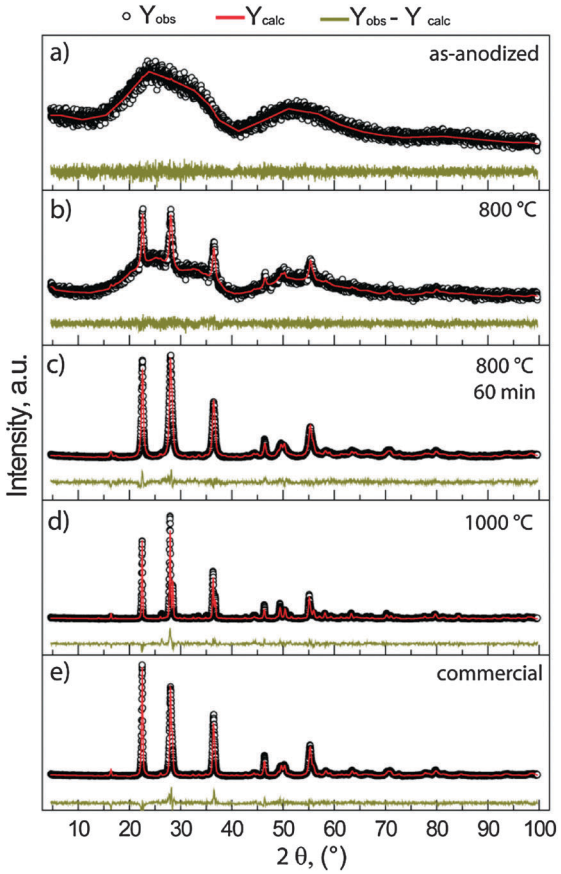

Fig. 2 XRD patterns and Rietveld refinement of Ta_2O_5 NTs: (a) as-anodized (b) calcined at 800 °C for 30 min (c) calcined at 800 °C for 60 min and (d) calcined at 1000 °C. (e) Commercial sample.

start parameters of Ta_2O_5 included the space group *P2mm* using the CIF information card (no. 9112). An amorphous phase was confirmed for the as-anodized sample (Fig. 2(a)). The XRD patterns of the NTs calcined at 1000 °C and 800 °C for 30 min and 60 min [Fig. 2(b)–(d)] showed a crystalline structure, which was identified as orthorhombic (JPCDS file 25-922).

Rietveld refinements were performed to investigate the crystal size of the calcined NTs and the commercial sample. The results are shown in Table 1. The crystallite size (Cs) increases from 15.5 to 52.4 nm as the treatment temperature increases from 800 to 1000 °C. In this temperature range, the growth rate of the crystallite size was 0.18 nm °C^{-1}. The degree of crystallinity (X_C)

Table 1 XRD and BET results for Ta_2O_5 NT materials

			BET		
Sample	C_S (nm)	X_C (%)	S_{BET} (m^2 g^{-1})	P_D (nm)	P_V (cm^3 g^{-1})
As-anodized	—	—	16.2	22.1	0.089
800 °C	15.4	11	13.2	248	0.080
800[a] °C	15.5	34	19.8	31.4	0.142
1000 °C	52.4	54	4.7	50.0	0.01
Commercial	49.0	37.0	4.7	22.1	0.089

X_C = crystallinity degree, C_S = crystal size, S_{BET} = specific surface area, P_D = pore diameter, and P_V = pore volume. [a] NTs calcined for 60 min.

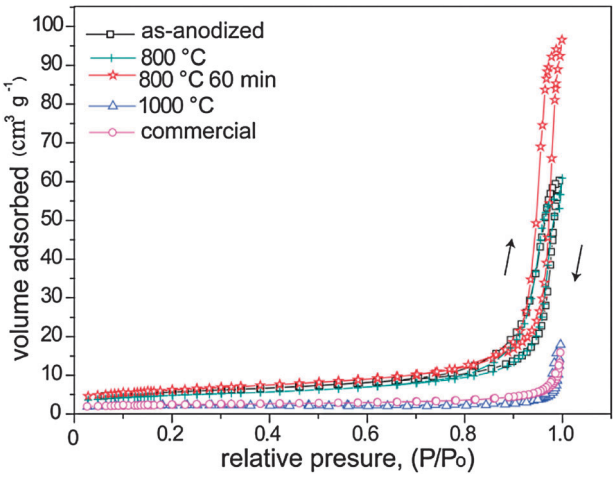

Fig. 3 Nitrogen adsorption isotherms of as-anodized Ta_2O_5 NTs and Ta_2O_5 NTs calcined at 800 and 1000 °C.

of the NTs, calcined at different temperatures, was determined from the ratio of the integral intensity of the crystalline contribution to the total intensity, see Table 1.[19] The commercial sample has a crystal size of 49 nm.

3.3 Specific surface area

The nitrogen adsorption–desorption isotherms of the Ta_2O_5 NTs are shown in Fig. 3. The specific surface area (S_{BET}) of 16.2, 13.2, 19.8, 4.7, and 4.7 m^2 g^{-1} was found for the as-anodized, calcined at 800 for 30 and 60 min, calcined at 1000 °C for 30 min, and commercial samples, respectively (Table 1).

Fig. 3 shows isotherms of the as-prepared and calcined NTs. A very low amount of N_2 was adsorbed at relative pressure of up to 0.8 P/P_0, which corresponds to nitrogen condensation in meso/macropores. The drastic increase in adsorption above the relative pressure of 0.8 P/P_0 suggests an important increase in the specific surface area and pore size distribution (Table 1).

3.4. FTIR study

Fig. 4 shows FTIR spectra of the prepared materials. As expected, Ta–O and Ta–O–Ta stretching vibration modes in 600–700 cm^{-1} were observed and some additional bands in 900–1000 cm^{-1} range were detected. These originated from the sub-oxide species present on the Ta_2O_5 NT surface.[20,21] They are also present in the FTIR spectra of the commercial sample.

The as-anodized material and the sample calcined at 800 °C for 30 min exhibited a characteristic band for the stretching vibration modes originated from sulfate ions at 1200 cm^{-1}.[22] The samples calcined at 800 °C for 60 min and at 1000 °C did not show bands in the 1100–1200 cm^{-1} region. It could be concluded that high temperature and a long time of calcination removed the sulfate ions that were present on the surface after preparation and remained also after calcination at 800 °C for 30 min. These results are in good agreement with the XPS data (see below), which showed the presence of S on the surface only for as-anodized material and the sample calcined at 800 °C for 30 min.

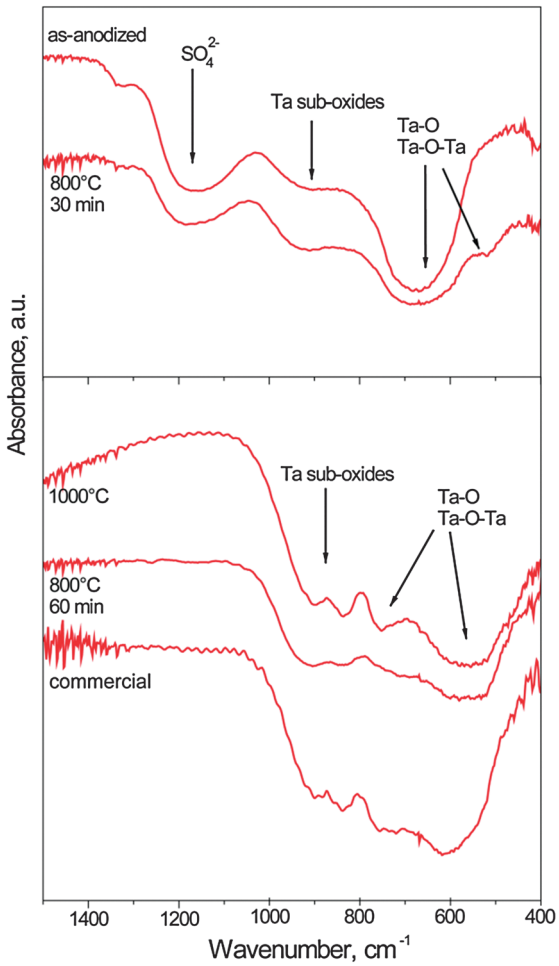

Fig. 4 FTIR spectra of Ta_2O_5 NTs as-anodized, calcined at different temperatures and the commercial sample.

3.5 XPS studies

X-ray photoelectron spectroscopy (XPS) is a powerful tool for determining the chemical composition and oxidation degrees of components present on the catalyst surface.

First, the XPS measurements were used to monitor the presence of residual contaminants at the surface after the preparation step and after thermal treatment. The S and F atoms from H_2SO_4 and HF used during material preparation should be easily detected by XPS on the as-anodized sample. Indeed, S and F (the S2p and F1s spectra are not shown here) were detected on the fresh amorphous Ta_2O_5 NT sample (before calcination). When the material was calcined at 800 °C for 30 min, some residual S was also detected. After the calcination at 800 °C (60 min) and 1000 °C (30 min), the S2p (at 168.45 eV) and F1s (at 684.29 eV) peaks disappeared, indicating the complete removal of the contaminants from the surface of Ta_2O_5 NTs. Molar concentrations of S and F are given in Table 2. Second, a quantitative analysis was performed for C1s, O1s, F1s, S2p, and Ta4f peaks for all catalysts. The results are presented in Table 2.

All samples showed carbon contamination. The decomposition of the C1s peak was performed using the methods reported

Table 2 XPS results of the calcined and as-anodized Ta_2O_5 NT samples

	XPS (%)				
Sample	Ta4f	O1s	C1s	S2p	F
As-anodized	16	47	26	6	5
800 °C	19	43	37	3	—
1000 °C	15	37	48	—	—
800[a] °C	21	46	33	—	—
Commercial	22	44	34	—	—

[a] NTs calcined for 60 min at 800 °C.

in the literature.[23] Three components were taken into account: one **C**–[C, H] contribution plus other two contributions corresponding to oxygenated carbon species (**C**–O_x = –**C**–OH + [C–(**C**=O)–OC]).

The O1s peak can be decomposed into two O1s components, the main one at about 529.7 eV was attributed to oxygen in tantalum oxide, and the other O1s small component at higher binding energy (530.9 eV) was attributed to O bound to carbon.

Very interesting observations were made in the case of the Ta4f peak. As shown in Fig. 5, the Ta4f peak of the amorphous sample (before calcination) could be decomposed into five main components. Two $4f_{7/2}$ and $4f_{5/2}$ peaks with corresponding binding energy of 26.06 and 27.96 eV originated from Ta^{5+} (Ta_2O_5 oxide). Two other small peaks observed at 22.60 and 24.50 eV could be assigned to the Ta^{2+} components. One additional peak at 29.20 eV

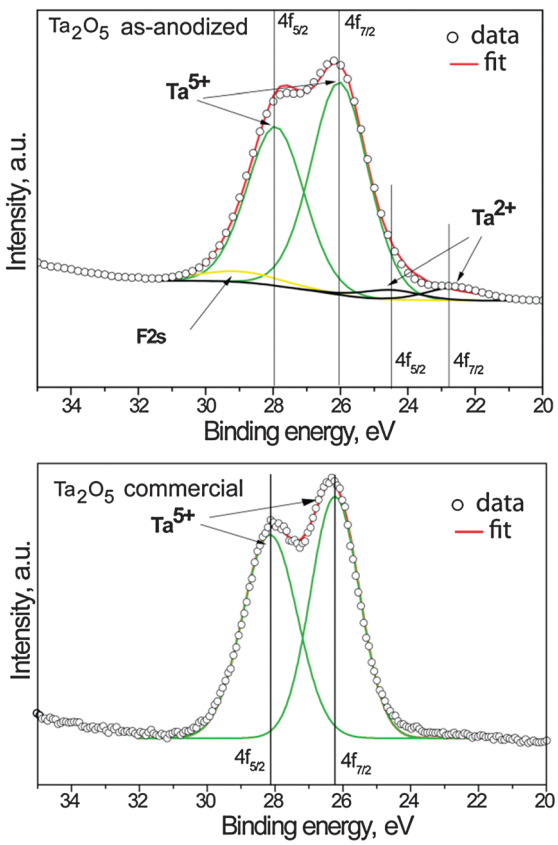

Fig. 5 XPS spectra of Ta4f and F2s regions for as-anodized Ta_2O_5 NTs and the commercial sample.

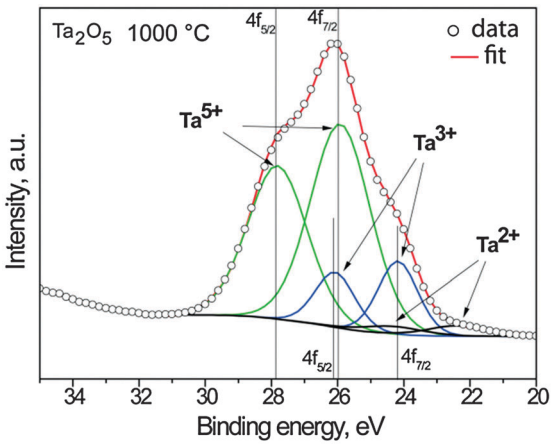

Fig. 6 XPS spectra of the Ta4f region for Ta_2O_5 NTs calcined at 1000 °C.

could be assigned to the F contamination (F2s peak). Fig. 5 also shows that the Ta^{5+} component was the only phase detected in the XPS 4f region in the commercial material.

The XPS spectra of the calcined samples (Fig. 6 and 7) differ from the spectrum of the as-anodized sample and the XPS spectra of the 4f peak could be decomposed into six main components.

The sample calcined at 1000 °C (Fig. 6) showed two high energy peaks at 26.00 and 27.90 eV corresponding to $4f_{7/2}$ and $4f_{5/2}$ components of Ta^{5+} and four low energy peaks at 22.40 and 24.17 eV assigned to the $4f_{7/2}$ peaks of Ta^{3+} and Ta^{2+}, respectively, and at 26.07 and 24.30 eV assigned to the $4f_{5/2}$ components of Ta^{3+} and Ta^{2+}. The shift in binding energy as compared to the amorphous sample (0.2 eV) could be due to the different crystal structure of the calcined material and the different particle size.

The samples calcined at 800 °C for 30 and 60 min (Fig. 7) showed two high energy peaks at 26.16 and 28.06 eV corresponding to the $4f_{7/2}$ and $4f_{5/2}$ peaks of Ta^{5+}. These values fit well with the binding energy for bare Ta^{5+} oxide reported in the literature[24–26] and with the binding energy observed in the amorphous sample and the sample calcined at 1000 °C (Table 4). However, the low energy peaks at 25.36 and 27.26 eV differ from those observed for the sample calcined at 1000 °C. A large shift of about 1.19 eV in binding energy suggests a different oxidizing state for tantalum. It should be assigned to the $4f_{7/2}$ and $4f_{5/2}$ peaks of Ta^{4+} rather than to Ta^{3+}. Two other low energy peaks observed in the XPS spectra at 22.33 and 24.23 correspond to the $4f_{7/2}$ and $4f_{5/2}$ peaks of Ta^{2+} already observed for the as-anodized sample and the sample calcined at 1000 °C.

3.6 Catalytic CO oxidation

The CO oxidation reaction was used to study the catalytic activity of the prepared Ta_2O_5 NTs. The catalytic experiments were performed in a continuous-flow reactor with a feed gas composition of 1.75 vol% CO, 7 vol% O_2, and Ar as the balance gas. It was passed through the catalytic bed at a total flow rate of 100 mL min^{-1}. The reactions were carried out without any pretreatment of the samples. After a series of catalytic experiments, both the calcined and amorphous Ta_2O_5 NTs were found to present relatively good catalytic activity (Fig. 8). However, some significant differences were observed in the catalytic behavior of the amorphous and crystalline NTs as described in Table 3. The catalytic activity of the NTs was also compared with the commercial Ta_2O_5 nanopowder provided by Sigma Aldrich.

The amorphous NTs and the commercial sample showed the lowest catalytic activity. Both samples showed a conversion of CO starting at 200 °C and reaching total conversion at 438 °C (entries 1 and 5, Table 3). The NTs calcined at 1000 °C showed higher activity than the amorphous and commercial materials.

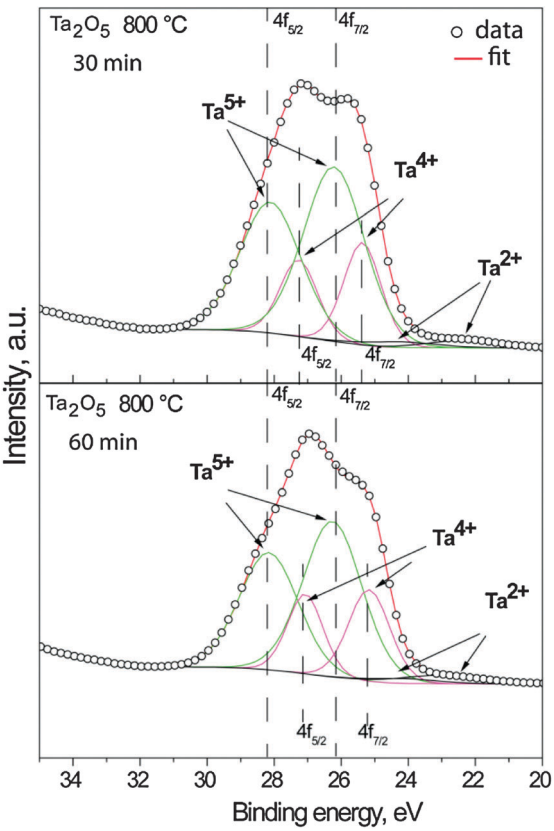

Fig. 7 XPS spectra of the Ta4f region for Ta_2O_5 NTs calcined at 800 °C for 30 and 60 min.

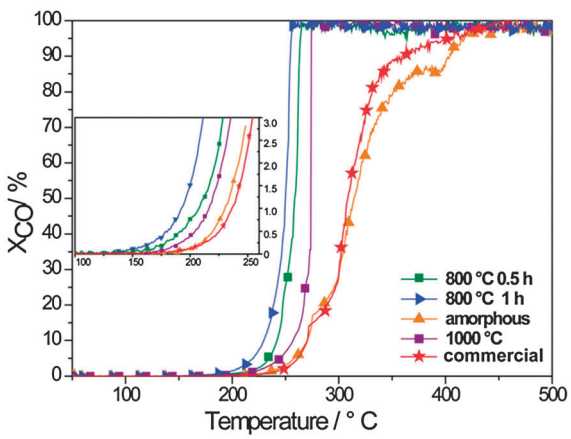

Fig. 8 CO conversion as a function of temperature over tantalum oxide.

Table 3 Catalytic activity of Ta_2O_5 NTs in the CO oxidation reaction

Entry	Ta_2O_5 catalyst	T_{ic} [a] (°C)	$T_{100\%}$ [b] (°C)	Conversion CO at 259 °C (%)	Rate[c]
1	As-anodized	200	438	5	0.18
2	800 °C (30 min)	169	265	52	1.58
3	1000 °C	180	278	11	0.38
4	800 °C (60 min)	157	259	100	3.38
5	Commercial	200	436	5	0.18

[a] Temperature of initial conversion. [b] Temperature of 100% of CO conversion. [c] Reaction rate expressed in $mmol_{CO}\ g^{-1}\ s^{-1}$.

The CO conversion started at 180 °C and 100% of conversion was reached at 278 °C (entry 3, Table 3). Both Ta_2O_5 NTs calcined at 800 °C showed a similar behavior to that of the NTs calcined at 1000 °C. They also showed an enhanced catalytic activity at lower temperature. The catalyst calcined at 800 °C for 30 min showed an initial temperature of 169 °C and the highest conversion was achieved at 265 °C. The best catalytic behavior was found for the material calcined at 800 °C for 60 min. This catalyst showed CO conversion starting at 157 °C and total conversion was achieved at 259 °C (entry 4, Table 3).

Significant differences were observed in the specific rate of the CO oxidation reaction expressed per gram of the catalyst (Table 3). At 259 °C ($T_{100\%}$ for most active catalyst), the highest rate was observed for the sample calcined at 800 °C for 60 min. A smaller but still higher rate was also observed for the sample calcined at 800 °C for 30 min. In contrast, the amorphous and crystallized samples (calcined at 1000 °C) had rates that were relatively low, at about 0.18 and 0.38 $mmol_{CO}\ g^{-1}\ s^{-1}$, respectively. The NTs calcined at 800 °C for 60 min are the most promising catalysts since the catalytic activity for the reaction with these materials was 9 and 19 times superior to the activity of those calcined at 1000 °C and amorphous nanotubes, respectively. All calcined Ta_2O_5 NT catalysts were more active than the commercial Ta_2O_5. The amorphous as-anodized NTs showed catalytic activity equal to the commercial Ta_2O_5 (see Fig. 8).

The NTs calcined at 800 °C (60 min) proved to be the most active catalysts, with the lowest temperatures of initial and complete conversion of CO, so the stability of this material was investigated under the CO oxidation reaction conditions for a long time-on-stream. The stability of the catalyst was studied at two temperatures: at 240 °C, with the conversion lower than 10%, and at 300 °C, with 100% conversion. Fig. 9 shows that the catalyst was very stable, remaining active for nearly 30 hours with less than 10% loss of the activity at 300 °C and without any loss of activity at 240 °C.

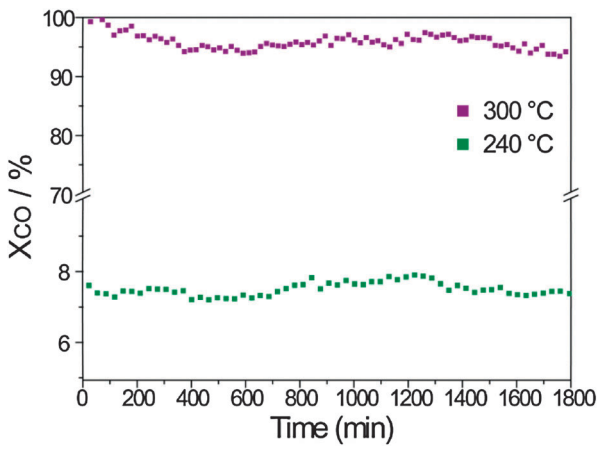

Fig. 9 Temporal stability of the CO oxidation reaction *versus* time-on-stream over Ta_2O_5 NTs calcined at 800 °C (60 min) at 240 °C and 300 °C.

4 Discussion

Recent studies have reported the successful application of anodization techniques for the preparation of homogeneous Ta_2O_5 NTs with a high degree of morphology control.[2,18,27] As-anodized Ta_2O_5 NTs have an amorphous structure and they generally need to be crystallized by calcination above 800 °C. In the present study, amorphous NT samples were crystallized by carefully calcining in an air atmosphere for 30 and 60 min at 800 °C, and 1000 °C for 30 min just after the anodization. Table 1 shows that the crystallinity of Ta_2O_5, determined by XRD, increased with both the temperature and the duration of calcination. The effect of calcination temperature on the morphology of Ta_2O_5 NTs has recently been studied.[19] Temperatures below of 800 °C yield NTs that showed amorphous character; the crystallization started only above 800 °C. The change in the NT morphology above 800 °C is due to the growth of crystals and grain boundaries on the surface of the material, as shown in Fig. 1. The Ta_2O_5 NTs calcined at 800 °C for 30 min retained their original tubular (as-anodized) morphologies. After calcination at 800 °C for 60 min, small holes and grain boundaries were observed. After calcination at 1000 °C, the nanotubular morphology was completely lost, and the tubes were converted into interconnected nanoparticles.

The XRD method is not sufficiently sensitive to detect small amounts of a given phase, and in the case of extreme similarity in crystal structure between two phases, it is impossible to differentiate them. An intergradation, in which different oxide phases coexist at a certain proportion, must exist. The Results section indicates that the XRD patterns of crystalline samples showed the presence of only one orthorhombic Ta_2O_5 phase. This confirms that Ta_2O_5 (Ta^{5+}) is a dominating phase but does not exclude the presence of other phases. The existence of other phases could be observed in the FTIR study. All Ta_2O_5 samples presented absorption peaks of Ta–O at 600–700 cm^{-1}. Moreover two peaks could be observed in the 900–1000 cm^{-1} range, associated with the tantalum sub-oxides. The FTIR studies also allowed confirmation of the presence of sulfate ions on the surface of the amorphous sample and the sample calcined at 800 °C for 30 min. After 60 min calcination at 800 °C, the sulfates could be completely removed from the surface.

The modification of amorphous Ta_2O_5 material *via* high temperature calcination changed the adsorption isotherm and significantly influenced the BET surface area. The most significant changes in the BET surface area were observed when the amorphous material was calcined at 1000 °C. The specific

surface area decreased from 16.2 to 4.7 $m^2\ g^{-1}$. It could be concluded that high temperature treatment allows high crystallinity of the material to be attained, but it drastically reduces the specific surface area due to the collapse of the nanotubular structure. In contrast, a lower temperature of treatment (800 °C for 60 min) permits the preservation of nanotubes with a high degree of crystallinity and a relatively high surface area (Table 1).

The catalytic activity of the Ta_2O_5 NTs was studied with respect to CO oxidation. The material with better catalytic activity proved to be the NTs calcined at 800 °C for 60 min. This material presented the highest specific surface area and pore volume, while the other materials did not follow any tendency with these parameters. The NTs calcined at 1000 °C are active as catalysts in the CO oxidation, even at the temperatures lower than 200 °C. Furthermore, they had the lowest specific surface area and pore volume, due to the effect of calcination at 1000 °C, which leads to the formation of large crystallites (crystallite size of 52.4 nm). The amorphous NTs exhibited similar values of S_{BET} and pore volume to those of the NTs calcined at 800 °C. Nevertheless, the catalytic activities of the amorphous and commercial materials were considerably inferior to those of the calcined samples.

Thus, the different activities of the prepared materials must be governed by factors other than the physical characteristics of the Ta_2O_5 NTs alone. For this reason, a detailed study of the active surface was performed by XPS analysis. This study revealed several important differences for each catalyst. As shown in Table 4, different species of tantalum oxide are present on the surface. The amorphous NTs have almost exclusively Ta^{5+} at the surface (94.31%). This composition differed for calcined materials, varying from 77.6 to 67.2% for the 1000 °C and 800 °C (60 min) samples, respectively.

It could be concluded that the catalytic activity of the Ta_2O_5 NTs depends on the composition of the surface. Indeed, as shown in Table 4, the content of active Ta^{4+} and Ta^{3+} phases differs for all samples. The highest activity was observed for the catalyst calcined at 800 °C for 60 min. This sample also showed the highest concentration of the Ta^{4+} surface species, as evidenced from the XPS study. The concentration of Ta^{4+} surface species varied with the time of calcination in the two samples calcined at 800 °C. Since the two most active catalysts contain Ta^{4+} species on the surface, this confirmed that this phase was most likely responsible for the high catalytic activity of these materials as compared to the amorphous material and the sample calcined at 1000 °C. The available literature confirms that the Ta^{4+} phase is very active in photocatalysis. Indeed, Ta^{4+} in bulk $NaTaO_3$ material greatly narrows its band gap from 3.94 to 1.70 eV and thus extends its photo-response from the UV into the visible light region, which leads to enhanced visible-light photocatalytic activity for water splitting and dye degradation.[26] This also suggests that chemically active, sub-stoichiometric (surface) defects promote CO oxidation.

Table 4 XPS results of the Ta4f region for Ta_2O_5 NTs materials

	Ta^{5+} ($4f_{7/2}$)		Ta^{4+} ($4f_{7/2}$)		Ta^{3+} ($4f_{7/2}$)		Ta^{2+} ($4f_{7/2}$)	
Sample	BE (eV)	%	BE (eV)	%	BE (eV)	%	BE (eV)	%
As-anodized	26.06	94.31	—	—	—	—	22.60	5.69
800 °C	26.16	70.93	25.36	25.52	—	—	22.33	3.55
1000 °C	26.00	77.62	—	—	24.17	18.43	22.40	3.95
800[a] °C	26.26	67.21	25.18	27.54	—	—	22.93	5.15
Commercial	6.23	100	—	—	—	—	—	—

[a] Ta_2O_5 NTs calcined for 60 min at 800 °C in an air atmosphere.

It is worth noting that these active species should be considered only as supra-surface species. They are formed on the surface and are not present in the bulk material. The results in this study clearly indicated a leading role for the Ta^{4+} active species in CO oxidation. However, due to the difficulties in controlling the whole catalyst surface, no direct evidence could be obtained for the active site location. Oxidation of CO occurs by active oxygen adsorbed onto the surface. This active oxygen site should be formed from the dissociation of molecular oxygen on metal atoms or oxygen vacancies. In the case of semiconductor oxides such as Ta_2O_5, different vacancies on the surface could possibly originate from differences in the crystallization process. It could be concluded that oxygen can adsorb and dissociate on the support (on Ta sub-oxides species) and facilitate the reaction. A possible charge transfer from the reducible oxide support, such as Ta_2O_5, to the adsorbed CO molecule could also play an important role in this reaction.

Conclusions

The most important outcome of this study is the confirmation of the dependence of the catalytic activity on the presence of Ta^{4+} and Ta^{3+} on the catalyst surface. Ta^{4+} was found to be the most active phase in the case of Ta_2O_5 NT catalysts. The Ta^{3+} phase is also active but at a higher temperature if compared to the Ta^{4+} phase. It is clear that Ta^{4+} and Ta^{3+} originated from the high temperature treatment and they should not be considered as a part of the bulk oxide. They are part of the supra-surface species. The formation of these species could be expected to occur on the surface during calcination and not in the bulk structure. The results showed the importance of the XPS study for determining the exact composition of the catalyst surface. Moreover, catalytic activity was found to depend on the surface Ta^{4+} cation content. The Ta^{4+} phase would appear to play a leading role in the CO oxidation mechanism of Ta_2O_5 oxide catalysts. In the present study, Ta_2O_5 nanotubes are shown to have higher catalytic activity in CO oxidation than do CeO_2–Al_2O_3 mixed oxides,[16] which indicates that Ta_2O_5 NTs have high potential for application as a catalyst material.

Acknowledgements

The authors are grateful for the financial support offered by the Brazilian agencies FAPESP, TWAS and CNPq and the University of São Paulo through the NAP-CatSinQ (Research Core in Catalysis and Chemical Synthesis). Our thanks are also extended to the National Synchrotron Light Laboratory (LNLS)

for the use of their conventional XPS equipment and Dr Heberton Wender and Dr Daniela Coelho de Oliveira for conducting the XPS measurements.

Notes and references

1 K. M. Parida, S. K. Mahanta, S. Martha and A. Nashim, *Int. J. Energy Res.*, 2013, **37**, 161–170.
2 R. V. Gonçalves, P. Migowski, H. Wender, D. Eberhardt, D. E. Weibel, F. v. C. Sonaglio, M. J. M. Zapata, J. Dupont, A. F. Feil and S. R. Teixeira, *J. Phys. Chem. C*, 2012, **116**, 14022–14030.
3 K. M. Parida, S. K. Mahanta, S. Martha and A. Nashim, *Int. J. Energy Res.*, 2011, **37**, 161–179.
4 A. Kudo and Y. Miseki, *Chem. Soc. Rev.*, 2009, **38**, 253–278.
5 H. Kato and A. Kudo, *Catal. Today*, 2003, **78**, 561–569.
6 H. Kato and A. Kudo, *Chem. Phys. Lett.*, 1998, **295**, 487–492.
7 Y. Noda, B. Lee, K. Domen and J. N. Kondo, *Chem. Mater.*, 2008, **20**, 5361–5367.
8 M. Ziolek, I. Sobczak, P. Decyk and L. Wolski, *Catal. Commun.*, 2013, **37**, 85–91.
9 M. Trejda, A. Wojtaszek, A. Floch, R. Wojcieszak, E. M. Gaigneaux and M. Ziolek, *Catal. Today*, 2010, **158**, 170–177.
10 M. Trejda, A. Wojtaszek, A. Floch, R. Wojcieszak, E. M. Gaigneaux and M. Ziolek, *Stud. Surf. Sci. Catal.*, 2010, **175**, 445–448.
11 A. V. Grigorieva, E. A. Goodilin, K. L. Dubova, T. A. Anufrieva, L. E. Derlyukova, A. S. Vyacheslavov and Y. D. Tretyakov, *Solid State Sci.*, 2010, **12**, 1024–1028.
12 A. V. Grigorieva, E. A. Goodilin, L. E. Derlyukova, T. A. Anufrieva, A. B. Tarasov, Y. A. Dobrovolskii and Y. D. Tretyakov, *Appl. Catal., A*, 2009, **362**, 20–25.
13 A. Jasik, R. Wojcieszak, S. Monteverdi, M. Ziolek and M. M. Bettahar, *J. Mol. Catal. A: Chem.*, 2005, **242**, 81–90.
14 R. Wojcieszak, S. Monteverdi, M. Mercy, I. Nowak, M. Ziolek and M. M. Bettahar, *Appl. Catal., A*, 2004, **268**, 241–253.
15 K. An, S. Alayoglu, N. Musselwhite, S. Plamthottam, G. Melaet, A. E. Lindeman and G. A. Somorjai, *J. Am. Chem. Soc.*, 2013, **135**, 16689–16696.
16 P. A. Deshpande, S. T. Aruna and G. Madras, *Catal. Sci. Technol.*, 2011, **1**, 1683–1691.
17 J. Rodriguezcarvajal, *Physica B*, 1993, **192**, 55–69.
18 N. K. Allam, X. J. Feng and C. A. Grimes, *Chem. Mater.*, 2008, **20**, 6477–6481.
19 R. V. Goncalves, P. Migowski, H. Wender, A. F. Feil, M. J. M. Zapata, S. jadoon, F. Bernardi, G. Azevedo and S. R. Teixeira, *CrystEngComm*, 2014, **16**, 797–804.
20 J.-Y. Zhang, B. Lim and I. W. Boyd, *Appl. Surf. Sci.*, 2000, **154–155**, 382–386.
21 J.-Y. Zhang, B. Lim and I. W. Boyd, *Thin Solid Films*, 1998, **336**, 340–343.
22 M. Hallquist, D. J. Stewart, S. K. Stephenson and R. Anthony Cox, *Phys. Chem. Chem. Phys.*, 2003, **5**, 3453–3463.
23 V. G. Baldovino-Medrano, B. Farin and E. M. Gaigneaux, *ACS Catal.*, 2012, **2**, 322–336.
24 K. Wang, Z. Liu, T. H. Cruz, M. Salmeron and H. Liang, *J. Phys. Chem. A*, 2010, **114**, 2489–2497.
25 Y. E. Roginskaya, O. V. Morozova, E. N. Loubnin, A. V. Popov, Y. I. Ulitina, V. V. Zhurov, S. A. Ivanov and S. Trasatti, *J. Chem. Soc., Faraday Trans.*, 1993, **89**, 1707–1715.
26 J. Wang, S. Su, B. Liu, M. Cao and C. Hu, *Chem. Commun.*, 2013, **49**, 7830–7832.
27 H. A. El-Sayed and V. I. Birss, *Nanoscale*, 2010, **2**, 793–798.

